Environmental Science & Technology

pubs.acs.org/est

Article

Evolution of Ozone Pollution in China: What Track Will It Follow?

Jia Guo, Xiaoshan Zhang,* Yi Gao, Zhangwei Wang, Meigen Zhang, Wenbo Xue, Hartmut Herrmann, Guy Pierre Brasseur, Tao Wang, and Zhe Wang*

Cite This: *Environ. Sci. Technol.* 2023, 57, 109−117

Read Online

ACCESS | Metrics & More | Article Recommendations | Supporting Information

ABSTRACT: Increasing surface ozone (O_3) concentrations has emerged as a key air pollution problem in many urban regions worldwide in the last decade. A longstanding major issue in tackling ozone pollution is the identification of the O_3 formation regime and its sensitivity to precursor emissions. In this work, we propose a new transformed empirical kinetic modeling approach (EKMA) to diagnose the O_3 formation regime using regulatory O_3 and NO_2 observation datasets, which are easily accessible. We demonstrate that mapping of monitored O_3 and NO_2 data on the modeled regional O_3−NO_2 relationship diagram can illustrate the ozone formation regime and historical evolution of O_3 precursors of the region. By applying this new approach, we show that for most urban regions of China, the O_3 formation is currently associated with a volatile organic compound (VOC)-limited regime, which is located within the zone of daytime-produced O_3 (DPO_3) to an 8h-NO_2 concentration ratio below 8.3 ($[DPO_3]/[8h\text{-}NO_2] \leq 8.3$). The ozone production and controlling effects of VOCs and NO_x in different cities of China were compared according to their historical O_3−NO_2 evolution routes. The approach developed herein may have broad application potential for evaluating the efficiency of precursor controls and further mitigating O_3 pollution, in particular, for regions where comprehensive photochemical studies are unavailable.

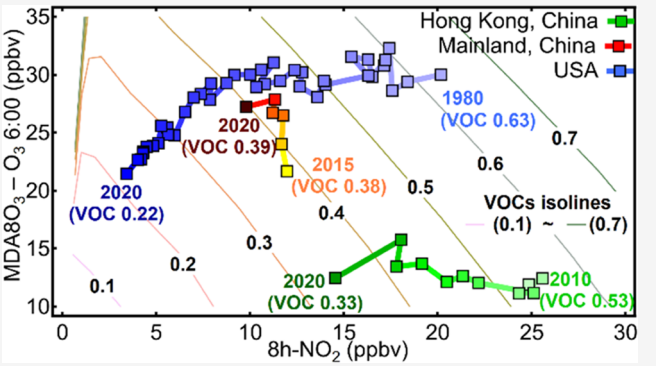

KEYWORDS: *ozone pollution, diagnosis approach, ozone formation regime, ozone−precursor relationship, air pollution mitigation*

INTRODUCTION

Ozone (O_3) has been regarded as a principal component of photochemical pollution in urban regions worldwide and has received continuous attention from both the scientific and regulatory communities due to its adverse impacts on human health, air quality, the climate, and the natural environment.[1,2] Tropospheric O_3 is produced from the sunlight-initiated photochemical processing of volatile organic compounds (VOCs), nitrogen oxides (NO_x), and, in a condition-dependent manner, carbon monoxide (CO), emitted from a vast variety of sources.[3,4] Although extensive efforts have been made to regulate O_3 precursor emissions worldwide,[5,6] O_3 concentrations reached very high levels, for example, in North America, before responding to control strategies developed and implemented over several decades.[7,8] Moreover, O_3 pollution continues to increase markedly in East Asia.[9−13] The nonlinear responses of O_3 formation to precursor emissions represent a major issue regarding O_3 pollution control, thus posing challenges to the formulation of a universal and efficient O_3 control strategy in regions with various chemical environments and regimes.[14,15]

Several approaches have been developed and utilized to identify O_3 formation regimes and their relationships with precursor emissions. These methods include onsite observations of indicator ratios,[16] emission-based air quality models,[13,17] relative incremental reactivity (RIR) assessments performed with observation-constrained models,[18] and the remote sensing of formaldehyde-to-NO_x ratios.[13,19] Most of these methods require sophisticated measurements, remote sensing data, accurate emission inventories, or detailed speciation information of emitted VOCs, while the O_3 and NO_2 data provided by regulatory monitoring networks are typically used to validate modeling results. In this work, we try to explore the utility of easily accessible NO_2 and O_3 monitoring datasets and develop an alternative approach analogous to the empirical kinetic modeling approach (EKMA) to obtain a classification scheme for diagnosing O_3 formation regimes in different regions. By visualizing the site-to-site variations and evolving routes of O_3−NO_2 relationships, we shed some light on the efficiency of precursor controls in different regions of China and the development of more cost-effective emission control strategies in the future.

Received: November 3, 2022
Revised: December 16, 2022
Accepted: December 16, 2022
Published: December 28, 2022

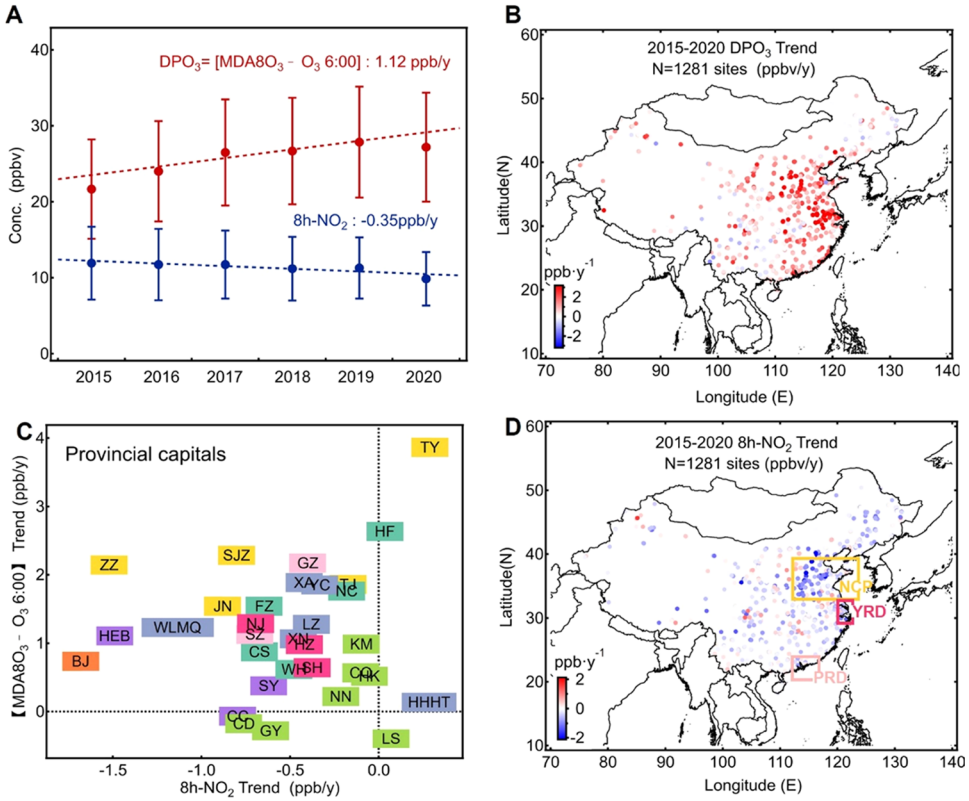

Figure 1. DPO_3 and 8h-NO_2 trends in China from 2015 to 2020. (A) Trends and linear regression of the nationally averaged DPO_3 and 8h-NO_2 concentrations. Spatial distribution of the annual increase rates of (B) DPO_3 and (D) 8h-NO_2 at the national monitoring sites (N = 1281) in China for the 2015−2020 period. (C) Quadrant distributions of the DPO_3 and 8h-NO_2 change rates in different provincial capital cities in China. The cities were marked using acronyms. The full names of the provincial capital cities and their locations on a map are also provided in Figure S2 in the Supporting Information.

MATERIALS AND METHODS

Continuous and standardized NO_2 and O_3 monitoring has been carried out at over 1200 sites in China by the National Environmental Monitoring Center (CNEMC) since 2013. This monitoring network provides long-term NO_2 and O_3 data at urban and suburban sites, covering different climatic regions of China. Hourly O_3 and NO_2 data recorded at national monitoring sites in China from January 2015 to December 2020 were obtained from the monitoring network website (http://106.37.208.233:20035). Historical O_3 and NO_2 monitoring data from Hong Kong and the United States were also incorporated into the analysis of this work. O_3 and NO_2 data recorded at the Air Quality Monitoring Stations (AQMS) in Hong Kong from 2010 to 2020 were obtained from the Hong Kong Environmental Protection Department (HKEPD) website. O_3 and NO_2 data collected by the United States Air Quality System (AQS) network from 1980 to 2020 were obtained from the Environmental Protection Agency (EPA) website. More detailed information on the sources and selection criteria of O_3 and NO_2 monitored data are described in the Supporting Information. In this work, we examined the relationship of 8h-NO_2 with the daytime-produced O_3 value (DPO_3 = $MDA8O_3$-O_3 ($6{:}00_{LT}$)). $MDA8O_3$ refers to the maximum daily 8 h average ozone. 8h-NO_2 is the average NO_2 in the same 8 h period of $MDA8O_3$. Daytime-produced O_3 value is defined as the difference between the $MDA8O_3$ value and the pre-sunrise O_3 measured at 6:00 am local time in the day. The metric DPO_3 ($MDA8O_3$-O_3) ($6{:}00_{LT}$) is used instead of $MDA8O_3$ for better conforming to the definition of the O_3 formation. As shown in Figure S1, the O_3 diurnal variations indicate small O_3 production at clean regions, such as the two background sites in Wyoming, US, whereas the $MDA8O_3$ levels cannot reflect the small O_3 local formation at these sites.

A zero-dimensional (0D) photochemical box model based on the Regional Atmospheric Chemistry Modeling (RACM) mechanism[20] was utilized to simulate the photochemical relationship between DPO_3 and 8h-NO_2 in a similar manner to the EKMA application in different regions and cities. We defined a default setting as a typical condition representing the average of meteorological and environmental situations. The default case was run under a moderate-condition setting in China, with assumptions of national average latitude 34 °N, temperature 290 K, relative humidity (RH) 50%, mixing layer height (MLH) varying from 200 to 1000 m, and on date of September 23rd (average solar radiation of a year). The speciation of anthropogenic VOCs (AVOCs) was derived from the Multiresolution Emission Inventory for China (MEIC) 2017 inventory,[21] which provides the emissions of the top-30 AVOC species with the highest ozone formation potential (OFP). The biogenic VOC (BVOC) emissions were classified into categories of *d*-limonene and other monoterpenes with two double bonds (LIM), monoterpenes with one double bond (API), and isoprene (ISO) categories, according to a previously published speciation scheme.[22] More detailed information on the model configuration and scenario settings are described in the Supporting Information.

https://doi.org/10.1021/acs.est.2c08205
Environ. Sci. Technol. 2023, 57, 109−117

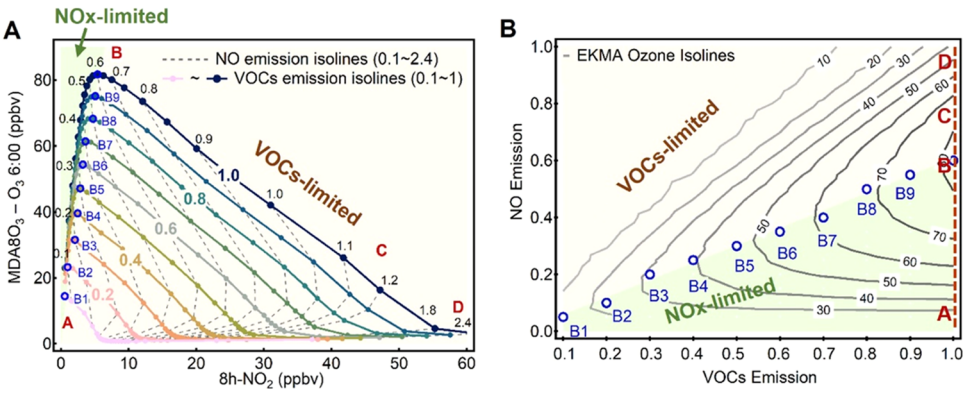

Figure 2. Relationship between DPO_3 (= $MDA8O_3$-O_3 6:00) and 8h-NO_2. (A, left panel) The modeled relationship between DPO_3 and 8h-NO_2 follows the A-to-D path along the VOC emission isolines (solid color isolines) with increasing NO_x emissions. Ten VOC emission settings (from 0.3×10^{-13} to 3.0×10^{-13} mol·cm^{-2}·s^{-1} in ten equal intervals) were prescribed and marked with the normalized ratios (0.1−1.0) on the isolines. The corresponding reactivity of VOC emissions, as represented by the equation $\sum$ Emission-$VOC_i \times MIR_i$, ranged from 0.146×10^{-10} to 1.46×10^{-10} gram O_3 cm^{-2}·s^{-1}. The NO_x emissions (addressed as NO emissions in the model) were prescribed from 0.05×10^{-12} to 2.4×10^{-12} mol cm^{-2} s^{-1} with 24 different values. Some representative NO_x emission isolines (gray dashed isolines) marked by the normalized ratios (0.1−2.4) are shown in the figure. The modeled data of default case to produce the diagram is listed in Table S3. (B, right panel) The modeled EKMA (empirical kinetic modeling approach) DPO_3 diagram of the default case, with the corresponding locations of the B points marked on the EKMA diagram. The red dashed line aligns with points A−B−C−D in panel B representing the VOC emission isoline shown in panel A. The O_3 formation regimes identified as NO_x-limited or VOC-limited are displayed in different background colors in panels A and B.

RESULTS AND DISCUSSION

DPO_3 and 8h-NO_2 Trends in China. Based on the monitoring dataset of China, we examined the changes in the annual DPO_3 and corresponding 8h-NO_2 at a total of 1281 selected CNEMC monitoring sites from 2015 to 2020 (Figure 1). The linearly regressed, nationally averaged increasing rate of DPO_3 was 1.12 ppb·y^{-1}, and the decreasing rate of 8h-NO_2 was −0.35 ppb·y^{-1} during 2015−2020 (Figure 1A). These results are consistent with previous observations obtained from individual photochemistry projects and those recorded at long-term background monitoring stations, where elevated ground O_3 levels over China have been widely reported.[9,10,23]

As shown in Figure 1, different cities have reflected different change directions and degrees in their DPO_3 and 8h-NO_2 levels. The increase in DPO_3 and decrease in 8h-NO_2 were both more noticeable in the cities in the North China Plain (NCP) and Eastern China than elsewhere in the country (Figure 1B,D). Some cities (e.g., Tianjin (TJ)) have experienced a slight 8h-NO_2 decrease but a large DPO_3 increase over the past six years, whereas cities such as Chengdu (CD) and Guiyang (GY) have shown minor decreases in DPO_3 relative to their substantial 8h-NO_2 reductions (Figure 1C). The O_3−NO_2 diagram approach, which was subsequently described, was utilized to further interpret the different O_3−NO_2 relationships of these Chinese cities.

O_3−NO_2 Diagram Approach. The "O_3−NO_2 diagram approach", like a transformed EKMA, traces the relationship between the modeled DPO_3, 8h-NO_2, and the precursor conditions on the O_3−NO_2 diagram modeled from the gas-phase 0D box model. The default case was performed under the typical condition of China. In addition to the default case, different scenario tests were conducted at various latitudes, temperatures, seasons, RH, MLH, and VOC speciation (see the Supporting Information).

By representing the calculated DPO_3 concentrations as the *Y*-values and 8h-NO_2 as the *X*-values in Figure 2A, the resulting VOC emission isopleth (color lines) depicts how photochemically produced O_3 and NO_2 respond to changes in NO_x emissions under fixed VOC emission conditions. The VOC emission isoline reflects the nonlinear response of O_3 formation to NO_x emissions and reveals a distinct transition of the O_3 formation sensitivity at turning points (B), at which the DPO_3 concentration increases (decreases) as NO_2 increases on the left (right) (Figure 2A). The role of these B points as sensitivity thresholds was also confirmed by their locations on the DPO_3 isopleth diagram modeled using the traditional EKMA and shown in Figure 2B. NO_x-limited regimes are represented by the left sides of the B points (Figure 2A), where the VOC isolines are densely arranged but do not overlap or cross (Figure S4). These closely spaced paths are consistent with the known insensitivity of O_3 formation to VOCs under NO_x-limited regimes. In contrast, VOC-limited regimes are represented by the right sides of the B points, with the low-to-high VOC emission isolines arranged from the bottom-left to the top-right (Figure 2A). The slopes of the C-to-B segments of the VOC isolines in Figure 2A represent the extent to which O_3 increases in response to NO_x mitigation under fixed VOC conditions in a VOC-limited regime.

We also examined the DPO_3−8h-NO_2 diagrams modeled under scenarios of different seasons, latitudes, temperatures, relative humidity as well as the VOC speciation (see Figure S5). The VOC isolines tend to be steeper during summer, during high temperatures, and at low latitude, and will be flatter or more inclined if all VOCs are alkenes or aromatics, respectively. In rare cases, the VOC isolines may be bent at the high NO_x emission ends (Figure S5); this condition is dependent on the time course of the NO+NO+O_2 = 2NO_2 reaction complementing the suppressed photochemical processes (Figure S6).

The positions of the division points (B) are important for distinguishing among different O_3 formation regimes. The influence of environmental factors (seasons, latitudes, temperatures, RH, VOC speciation, etc.) on the division point (B) locations was examined. The division points (B) of all of the examined Chinese scenarios were located in a quite narrow area when considering the possible factor ranges characterizing

https://doi.org/10.1021/acs.est.2c08205
Environ. Sci. Technol. 2023, 57, 109−117

Chinese cities (Figure 3), thus revealing the possibility of identifying the O_3 formation regime by directly referring to these B point locations. In the figure, the linear equation of $[DPO_3] = 8.3 \times [8h\text{-}NO_2]$ represents the "safe" boundary, indicating a VOC-limited regime with regard to the annual mean O_3–NO_2 relationship for most Chinese cities. For more accurate analysis, it is recommended that a localized DPO_3–8h-NO_2 diagram should be produced for a specific region or city, with the specialized meteorological condition and VOC speciation of this region/city.

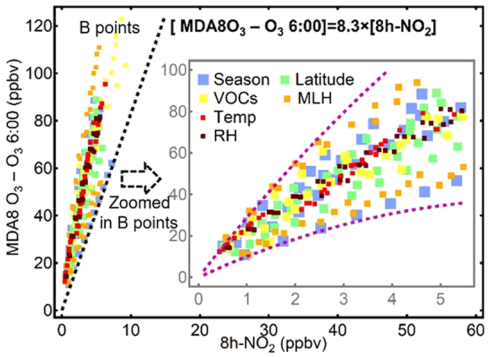

Figure 3. Sensitivity of the locations of the B points to the temperature, RH, season, latitude, MLH, and VOC speciation conditions. The black dashed line, represented by $[DPO_3] = 8.3 \times [8h\text{-}NO_2]$, indicates a safe boundary for VOC-limited regimes under various scenarios in China. The inset shows the expansion of the regime-transition region. The purple dashed lines represent the upper and lower bounds of the regime-transition region with regards to the annually averaged DPO_3 and 8h-NO_2 data characterizing Chinese cities, which were modeled under the southmost conditions (20 °N, 303 K, MLH 100–700 m) and northmost conditions (50 °N, 273 K, MLH 400–1000 m), respectively.

O_3 Formation Regimes and Historical Routes Response to Precursor Controls. We mapped the annually averaged DPO_3 and 8h-NO_2 data of the Chinese monitoring sites on the modeled O_3–NO_2 relationship diagram (Figure 4A). As shown in the figure, most of the measurement data were located to the right of the safe regime-transition boundary line $[DPO_3] = 8.3 \times [8h\text{-}NO_2]$, indicating VOC-limited O_3 formation regime. We also mapped the seasonal averaged DPO_3 and 8h-NO_2 data on modeled seasonal O_3–NO_2 relationship diagrams (Figure 5), which show similar results to the yearly averages. The patterns of the monitoring scatters and the predicted seasonal diagrams consistently depicted the varying characteristics of temperature and solar radiation across the seasons. Both the isolines and scatter distribution were steeper in the summer and flatter in the winter.

Previous measurements and modeling studies have generally suggested that ozone production is under VOC-limited regimes in urban and industrial regions but under NO_x-limited regimes in most rural areas in China.[9,13,24,25] The present work tends to suggest the dominance of VOC-sensitive O_3 formation regimes in the regions represented by the national monitoring stations. The DPO_3–8h-NO_2 scatterplot exhibits an evolving trend toward the upper-left direction with annually increasing O_3 values during the 2015–2020 period (Figure 4A). This evolution direction is consistent with the NO_x emission control efforts enacted in the country over the past five years. But referring to the location of the modeled safe boundary line $[DPO_3] = 8.3 \times [8h\text{-}NO_2]$, most of the Chinese sites still have a long way to go to reach NO_x-limited regimes though the significant NO_x emission control.

The United States (US) has suffered from high O_3 pollution for a long time, and the successful emission reductions in recent decades can provide insights into the potential evolution and control of O_3 pollution.[7,26] The annual average O_3 production and NO_2 data recorded by the US EPA monitoring network from 1980 to 2020 are depicted in Figure 4B, which shows the overall historical route of the USA's DPO_3–8h-NO_2 in the past few decades. The data clearly show an evolution toward the lower DPO_3 and NO_2 region moving toward the NO_x-limited regime. More sites have passed the transition point in recent years. Notably, concurrent decreases in O_3 and NO_2 were observed when the 8h-NO_2 value reached approximately 10 ppbv after 2000, but this should not be interpreted as the turning point to the NO_x-limited regime. Instead, these decreases are the result of the simultaneous successful control of NO_x and VOC emissions. By comparing the O_3 evolution route with the modeling results shown in

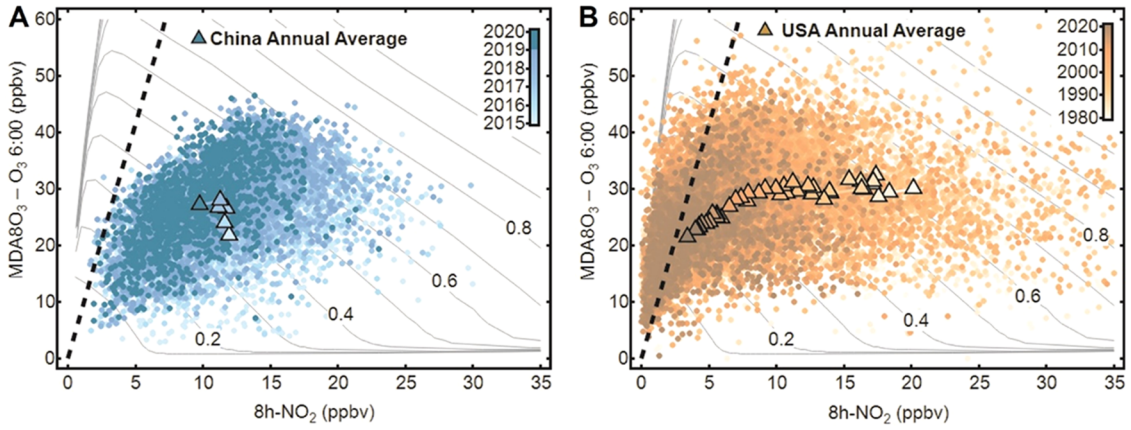

Figure 4. Annual DPO_3–8h-NO_2 data and evolving trends in China and USA. Locations of the annually averaged DPO_3–8h-NO_2 data recorded at (A) 1281 sites in China from 2015 to 2020 and at (B) monitoring sites in the USA from 1980 to 2020, superposed on the VOC emission isolines (0.1–1.0) derived under the default modeling conditions shown in Figure 2. The dots represent the annual average values at monitoring sites in China or the USA, and the triangles represent the national annual mean values at all sites in different years. The color scales indicate the year in which the data were measured.

https://doi.org/10.1021/acs.est.2c08205
Environ. Sci. Technol. 2023, 57, 109–117

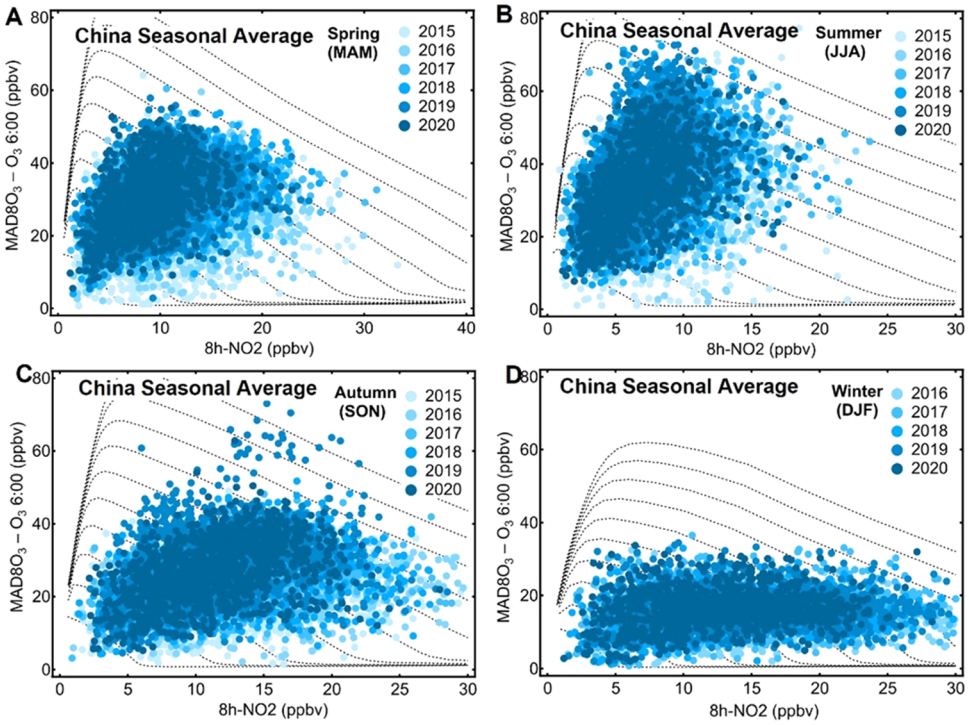

Figure 5. Graphs illustrating the locations of seasonally averaged DPO_3−8h-NO_2 data recorded at 1281 sites in China from 2015 to 2020 on modeled seasonal DPO_3−8h-NO_2 diagrams.

Figure 4B, the USA data exhibit a shift across approximately five VOC isolines since 1980. An estimated 65% reduction in VOCs and a 70% reduction in NO_x can be inferred based on the locations at which the VOC and NO_x isolines cross. According to the US EPA, national emissions (excluding biogenic and wildfires) of VOCs and NO_x were reduced by 60 and 70%, respectively, from 1980 to 2020 (https://www.epa.gov/air-trends/air-quality-national-summary). Though this semiquantitative estimation is associated with many uncertainties, including VOC speciation and meteorological condition differences between the countries, the trends and changing degrees estimated from the diagram generally match the emission inventory well.

In another direct and useful application of the diagram, we visualized the site-to-site variations and evolution routes of different cities/regions on the DPO_3−8h-NO_2 diagram (Figure 6). The locations of the Chinese provincial capitals on the diagram (Figure 6A) are consistent with current knowledge regarding the spatial distributions of NO_x and VOC pollution in China.[27,28] The highly industrialized and populated cities (e.g., cities in NCP, shown with a yellow background) are located in the upper-right quadrant of Figure 6A, suggesting that this highly polluted region experiences concurrently high NO_x and VOC emissions. In contrast, the relatively less-industrialized cities in southwestern China (green background) are generally located in the bottom-left quadrant of the diagram.

The evolving routes of different cities/regions shown on the diagram shed light on the historical precursor control strategies enacted in these cities/regions. As an example, we compared the evolving routes of the major cities in three most-developed regions in China shown in Figure 6B−D. The NCP, PRD, and YRD cities mostly showed steep DPO_3−8h-NO_2 tracks moving along the VOC emission isoline direction. Beijing and Hong Kong presented a relatively flat trace, crossing more VOC isolines and shifting leftward with a large 8h-NO_2 decrease but a small O_3 increase. This shift of Beijing toward the lower VOC isolines on the diagram suggests a reduction in VOC emissions of approximately 24% from 2015 to 2020. The O_3 pollution in Hong Kong is shown to be primarily VOC-limited, exhibiting an O_3 increasing trend overall throughout the last 20 years.[5] As shown in Figure 6D, the annual DPO_3−8h-NO_2 data recorded in Hong Kong from 2010 to 2020 moved leftward, exhibiting a slight increase in O_3 production but crossing two VOC emission isolines. This trend implies an approximate VOC reduction of 22% and a NO_x reduction of 24% from 2010 to 2018 in Hong Kong. This estimation agrees well with the emission inventory from HKEPD, in which 26 and 23% reductions during this period were, respectively, reported in VOCs and NO_x emissions,[29] though the estimation was made based on the assumption of default VOC speciation of China. We also compared the estimated precursor emissions at the 1281 sites from the DPO_3−8h-NO_2 diagram with the emission rates obtained from the MEIC for the same region (Figure S8). The general trend of the inferred emission conditions was consistent with the bottom-up emission inventory, thus imparting confidence in the capability of the DPO_3−8h-NO_2 approach for diagnosing O_3 formation and precursor controls in different regions.

It should be noted that this diagram approach would perform better on long-term historical analysis. This is because the utilized long-term observation dataset to some extent can overcome the short-time fluctuations and provide an overall diagnosis of the O_3−precursor relationship. For example, interannual variations of meteorology would impact the evolving trace of the monitoring data. In addition, the fast reduction in $PM_{2.5}$ concentrations in China in recent years could cause the near-surface radiation increase and reduce the heterogeneous aerosol sink of HO_2 radicals,[30,31] thus contributing to O_3 concentration increases and upward shifting

https://doi.org/10.1021/acs.est.2c08205
Environ. Sci. Technol. 2023, 57, 109−117

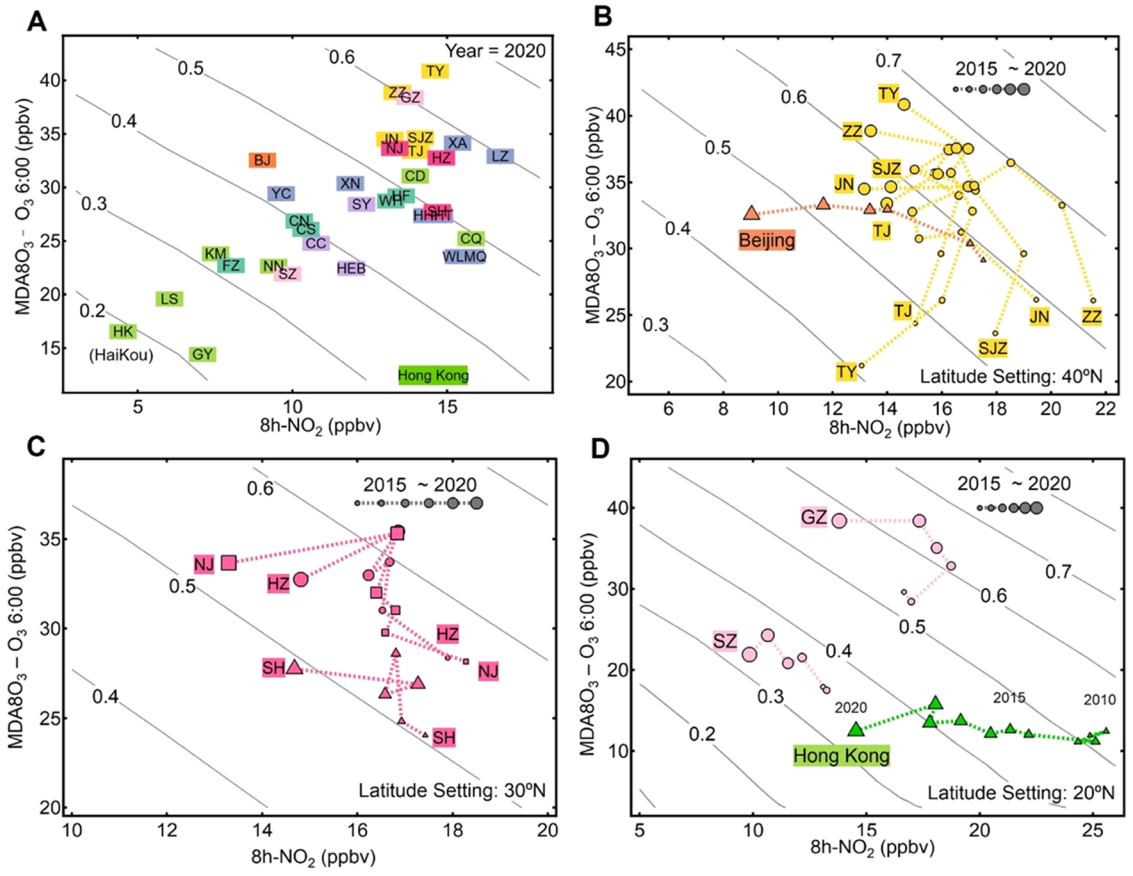

Figure 6. Annual DPO_3–8h-NO_2 locations and evolving trends in different regions and cities of China. (A) Annually averaged DPO_3–8h-NO_2 data in all provincial capital cities in China in 2020 superposed on the VOC emission isolines established under the default case. The cities are marked using acronyms and grouped in different colors, according to their locations in different regions of China, as in Figures 2 and S2. (B–D) Evolution of DPO_3–8h-NO_2 over the past decade in cities located in the major regions of China, superposed on the VOC emission isolines obtained from the average condition of each region. The coverage of the NCP, PRD, and YRD regions is described in Figure S7 in the Supporting Information. The marker size represents the annual data values obtained in different years.

of the DPO_3–8h-NO_2 data on the diagram. These factors cannot be distinguished from the modeled DPO_3–8h-NO_2 diagram and would bias the diagram-estimated emission changes over the years. In estimating the trend in precursors, long-term datasets have an advantage due to their ability to overcome fluctuations between years.

Future O_3 Pollution Mitigation in China. In view of the severe O_3 pollution in China, the government has implemented and planned aggressive control measures regarding the emissions of pollutant species. Thus, we evaluated the impacts of future precursor controls on O_3 pollution using the diagram estimation approach (Figure 7). The approach shows that a minimum reduction ratio (0.75:1.0) for VOC/NO_x is required to achieve nonincreasing O_3 production from the current annual levels. China's 14th five-year plan calls for reductions of more than 10% in both VOC and NO_x emissions by 2025 and emphasizes that the VOC reduction ratio should be no less than that of NO_x in polluted regions. This synergetic 10% reduction in VOC and NO emissions is estimated to decrease the photochemically produced annual O_3 concentration by approximately 2.0 ppbv (Figure 7A) and the summer O_3 production by 1.5 ppbv on the national average (Figure S9). Based on the locations of the present DPO_3–8h-NO_2 and the localized baseline for the NCP, YRD, and PRD regions, regional reduction effects were further investigated (Figure 7B–D). With a synergetic 10% reduction in both VOC and NO_x emissions, the anticipated decreases in DPO_3 would be 2.5, 2.6, and 0.5 ppbv for the NCP, YRD, and PRD regions, respectively. On the contrary, DPO_3 in Hong Kong may increase by 0.6 ppb under the same reduction scenario and will reduce only when a higher VOC reduction percentage can be achieved. The estimated DPO_3 levels will fall by 10.4, 10.5, and 9.2 ppbv in NCP, YRD, and PRD, if the NO_x and VOC emissions can be reduced by 10 and 20%, respectively. For the cases with only VOCs decreased by 20%, the predicted DPO_3–8h-NO_2 points would move downward along the NO_x isolines (gray dash lines in Figure 7), with the DPO_3 drops of 16.8, 16.3, 14.5, and 6.1 ppbv in NCP, YRD, PRD, and Hong Kong, respectively; meanwhile, the 8h-NO_2 level would likely rise.

Despite the fact that the O_3–NO_x–VOC sensitivity could vary across regions and seasons, the majority of recent studies suggest that VOC-targeted management is a more workable solution in China. For example, based on the WRF-CMAQ modeling, Wang et al. proposed that O_3 pollution mitigation in NCP, YRD, and PRD would be effective when the VOCs/NO_x reduction ratio is more than 2:1.[32] Another modeling study in PRD showed that a reduction ratio of VOC/NO_x more than 1:1 was necessary to accomplish synergetic control, and the best O_3 reduction was found for a VOC-only control scenario.[33] A recent study based on satellite retrievals also suggested that the ozone concentration in Beijing, Chengdu,

https://doi.org/10.1021/acs.est.2c08205
Environ. Sci. Technol. 2023, 57, 109–117

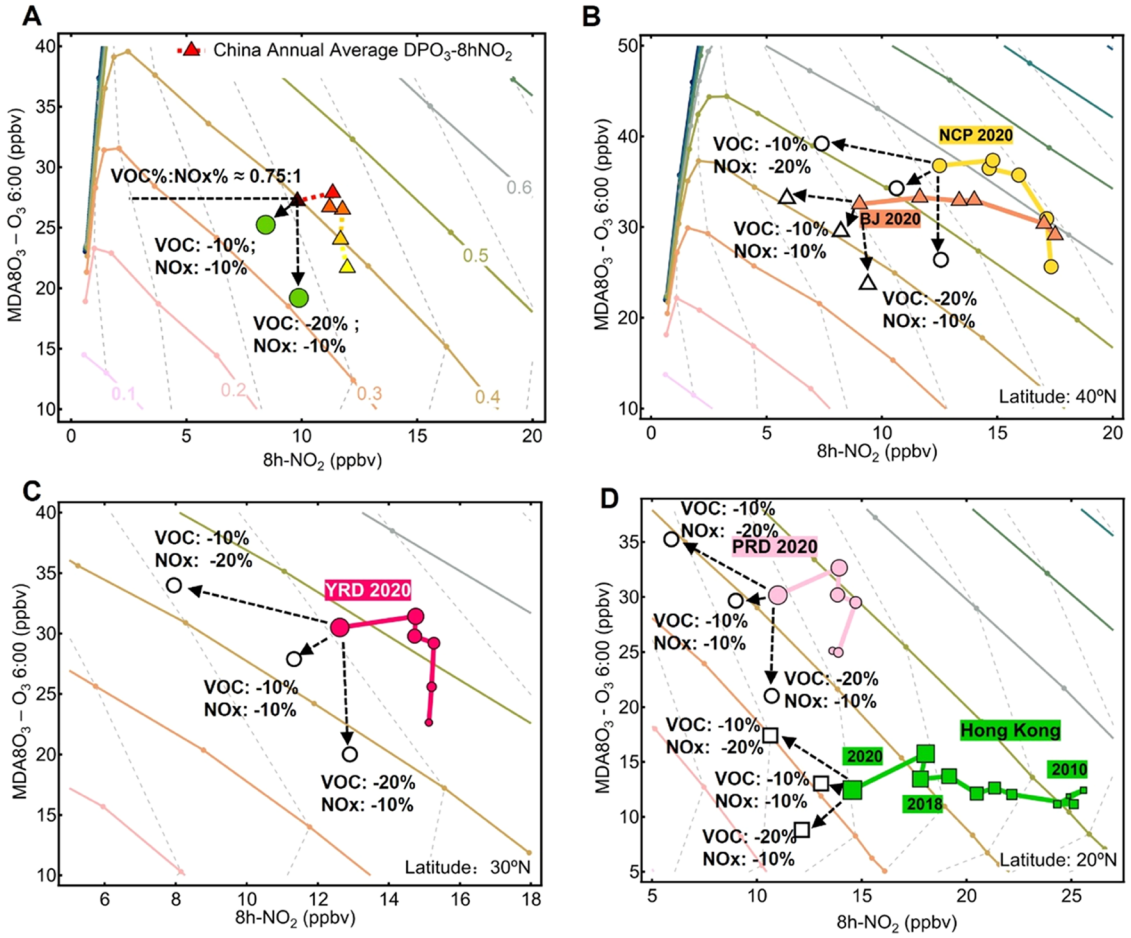

Figure 7. Prediction of DPO_3–8h-NO_2 changes under different VOC and NO_x emission control scenarios in China after 2020. (A) Estimated future changes in the national annual average DPO_3–8h-NO_2 level in China and (B–D) regions of NCP, YRD, and PRD in China under different emission–reduction scenarios in VOC and NO emissions. The regionally averaged data are superimposed on the VOC emission isolines (solid color lines) and NO emissions isolines (gray dashed lines) derived under the corresponding average condition of each region. The predicted locations and evolving traces of the annual DPO_3–8h-NO_2 levels under different VOC/NO_x control strategies or in different regions are shown in open markers and dashed arrows on the diagrams.

and Guangzhou would be significantly lowered if the reduction ratio of VOCs/NO_x is between 2:1 and 4:1.[34] These previous investigations, together with the present work, all highlighted that the basis for O_3 pollution management is an approximately 1:1 synergetic reduction of VOC and NO_x and that a ratio greater than 2:1 could contribute to significantly reduced O_3 levels.

In summary, the good performance on estimating the historical precursors controlling in the US and Hong Kong provides supporting evidence for the applicability of the DPO_3–8h-NO_2 diagram when addressing O_3 pollution and evolution in different regions. This robust and rapid classification approach, in which only the continuous NO_2 and O_3 measurement data were utilized, may have broad application potential in evaluating the precursor control effects and assisting in developing O_3 pollution mitigation strategies, in particular, for regions where comprehensive photochemical studies are unavailable. The historical evolution of air pollution in the US indicates that successfully controlling O_3 pollution is possible. Synergetic VOC and NO_x reduction and increasingly strict anthropogenic VOC control should be the primary focus at the present stage for controlling O_3 pollution in China.

■ ASSOCIATED CONTENT

Supporting Information

The Supporting Information is available free of charge at https://pubs.acs.org/doi/10.1021/acs.est.2c08205.

Including monitoring data sources, modeling settings, the data for default case isolines plotting (Table S3), other supporting figures (Figures S1–S9), and tables (Tables S1 and S2) (PDF)

■ AUTHOR INFORMATION

Corresponding Authors

Xiaoshan Zhang – *Key Laboratory of Urban and Regional Ecology, Research Center for Eco-Environmental Sciences, Chinese Academy of Sciences, Beijing 100085, China; University of Chinese Academy of Sciences, Beijing 100049, China;* orcid.org/0000-0001-6124-7806; Email: zhangxsh@rcees.ac.cn

Zhe Wang – *Division of Environment and Sustainability, The Hong Kong University of Science and Technology, Kowloon 999077 Hong Kong, China;* orcid.org/0000-0002-5627-6562; Email: z.wang@ust.hk

https://doi.org/10.1021/acs.est.2c08205
Environ. Sci. Technol. 2023, 57, 109–117

Authors

Jia Guo − *Key Laboratory of Urban and Regional Ecology, Research Center for Eco-Environmental Sciences, Chinese Academy of Sciences, Beijing 100085, China; University of Chinese Academy of Sciences, Beijing 100049, China;* Present Address: The Hong Kong University of Science and Technology, Kowloon 999077, Hong Kong, China

Yi Gao − *University of Chinese Academy of Sciences, Beijing 100049, China; State Key Laboratory of Atmospheric Boundary Layer Physics and Atmospheric Chemistry (LAPC), Institute of Atmospheric Physics, Chinese Academy of Sciences, Beijing 100029, China*

Zhangwei Wang − *Key Laboratory of Urban and Regional Ecology, Research Center for Eco-Environmental Sciences, Chinese Academy of Sciences, Beijing 100085, China; University of Chinese Academy of Sciences, Beijing 100049, China;* orcid.org/0000-0002-0516-4536

Meigen Zhang − *University of Chinese Academy of Sciences, Beijing 100049, China; State Key Laboratory of Atmospheric Boundary Layer Physics and Atmospheric Chemistry (LAPC), Institute of Atmospheric Physics, Chinese Academy of Sciences, Beijing 100029, China*

Wenbo Xue − *Center of Air Quality Simulation and System Analysis, Chinese Academy of Environmental Planning, Beijing 100012, China*

Hartmut Herrmann − *Atmospheric Chemistry Department (ACD), Leibniz Institute for Tropospheric Research (TROPOS), Leipzig 04318, Germany;* orcid.org/0000-0001-7044-2101

Guy Pierre Brasseur − *Department of Civil and Environmental Engineering, The Hong Kong Polytechnic University, Kowloon 999077 Hong Kong SAR, China; Environmental Modeling Group, Max Planck Institute for Meteorology, Hamburg 20146, Germany; Atmospheric Chemistry Observations and Modeling Laboratory, National Center for Atmospheric Research, Boulder, Colorado 80307, United States*

Tao Wang − *Department of Civil and Environmental Engineering, The Hong Kong Polytechnic University, Kowloon 999077 Hong Kong SAR, China*

Complete contact information is available at: https://pubs.acs.org/10.1021/acs.est.2c08205

Author Contributions

J.G., X.Z., and Z.W. designed the study; J.G. performed the modeling simulation and data analysis; J.G. and Z.W. led the manuscript writing with specific comments and edits from all other co-authors.

Notes

The authors declare no competing financial interest.

All data are available in the main text or Supporting Information. Correspondence and requests for further materials should be addressed to X.Z. (zhangxsh@rcees.ac.cn) and Z.W. (z.wang@ust.hk).

■ ACKNOWLEDGMENTS

The authors would like to acknowledge the China Ministry of Ecology and Environment, Hong Kong Environmental Protection Department, and the United States Environmental Protection Agency for the O_3 and NO_2 measurement data. They thank the Leibniz Institute for Tropospheric Research (TROPOS) for providing the source code (http://projects.tropos.de/capram) for the photochemical mechanism modeling. This work was supported by the National Key R&D Program of China (2016YFC0203200), the National Natural Science Foundation of China (NSFC) project (42122062 and 41605093), the Research Grants Council of Hong Kong Special Administrative Region (grant nos. T24/504/17-N and 16209022), and the Hong Kong Environment and Conservation Fund (project 125/2020).

■ REFERENCES

(1) Finlayson-Pitts, B. J.; Pitts, J. N. Tropospheric Air Pollution: Ozone, Airborne Toxics, Polycyclic Aromatic Hydrocarbons, and Particles. *Science* **1997**, *276*, 1045−1051.

(2) Akimoto, H. Global Air Quality and Pollution. *Science* **2003**, *302*, 1716−1719.

(3) Haagensmit, A. J. Chemistry and Physiology of Los-Angeles Smog. *Ind. Eng. Chem.* **1952**, *44*, 1342−1346.

(4) Crutzen, P. A discussion of the chemistry of some minor constituents in the stratosphere and troposphere. *Pure Appl. Geophys.* **1973**, *106*−*108*, 1385−1399.

(5) Wang, T.; Dai, J. N.; Lam, K. S.; Nan Poon, C.; Brasseur, G. P. Twenty-Five Years of Lower Tropospheric Ozone Observations in Tropical East Asia: The Influence of Emissions and Weather Patterns. *Geophys. Res. Lett.* **2019**, *46*, 11463−11470.

(6) Parrish, D. D.; Law, K. S.; Staehelin, J.; Derwent, R.; Cooper, O. R.; Tanimoto, H.; Volz-Thomas, A.; Gilge, S.; Scheel, H. E.; Steinbacher, M.; Chan, E. Long-term changes in lower tropospheric baseline ozone concentrations at northern mid-latitudes. *Atmos. Chem. Phys.* **2012**, *12*, 11485−11504.

(7) Parrish, D. D.; Zhu, T. Clean Air for Megacities. *Science* **2009**, *326*, 674−675.

(8) Cooper, O. R.; Langford, A. O.; Parrish, D. D.; Fahey, D. W. Challenges of a lowered U.S. ozone standard. *Science* **2015**, *348*, 1096−1097.

(9) Wang, T.; Xue, L. K.; Brimblecombe, P.; Lam, Y. F.; Li, L.; Zhang, L. Ozone pollution in China: A review of concentrations, meteorological influences, chemical precursors, and effects. *Sci. Total Environ.* **2017**, *575*, 1582−1596.

(10) Xu, X. B.; Lin, W. L.; Xu, W. Y.; Jin, J. L.; Wang, Y.; Zhang, G.; Zhang, X. C.; Ma, Z. Q.; Dong, Y. Z.; Ma, Q. L.; et al. Long-term changes of regional ozone in China: implications for human health and ecosystem impacts. *Elementa* **2020**, *8*, No. 409.

(11) Cooper, O. R.; Parrish, D. D.; Ziemke, J.; Balashov, N. V.; Cupeiro, M.; Galbally, I. E.; Gilge, S.; Horowitz, L.; Jensen, N. R.; Lamarque, J.-F.; et al. Global distribution and trends of tropospheric ozone: An observation-based review. *Elementa* **2014**, *2*, No. 000029.

(12) Wang, Y.; Gao, W.; Wang, S.; Song, T.; Gong, Z.; Ji, D.; Wang, L.; Liu, Z.; Tang, G.; Huo, Y.; et al. Contrasting trends of PM2.5 and surface-ozone concentrations in China from 2013 to 2017. *Natl. Sci. Rev.* **2020**, *7*, 1331−1339.

(13) Wang, N.; Huang, X.; Xu, J.; Wang, T.; Tan, Z. M.; Ding, A. Typhoon-boosted biogenic emission aggravates cross-regional ozone pollution in China. *Sci. Adv.* **2022**, *8*, No. eabl6166.

(14) Hallquist, M.; Munthe, J.; Hu, M.; Wang, T.; Chan, C. K.; Gao, J.; Boman, J.; Guo, S.; Hallquist, Å. M.; Mellqvist, J.; et al. Photochemical smog in China: scientific challenges and implications for air-quality policies. *Natl. Sci. Rev.* **2016**, *3*, 401−403.

(15) Ding, D.; Xing, J.; Wang, S.; Dong, Z.; Zhang, F.; Liu, S.; Hao, J. Optimization of a NOx and VOC Cooperative Control Strategy Based on Clean Air Benefits. *Environ. Sci. Technol.* **2022**, *56*, 739−749.

(16) Sillman, S. The use of NOy, H2O2, and HNO3 as indicators for ozone-NOx-hydrocarbon sensitivity in urban locations. *J. Geophys. Res.* **1995**, *100*, 14175−14188.

(17) Milford, J. B.; Russell, A. G.; McRae, G. J. A new approach to photochemical pollution control: implications of spatial patterns in pollutant responses to reductions in nitrogen oxides and reactive organic gas emissions. *Environ. Sci. Technol.* **1989**, *23*, 1290−1301.

(18) Cardelino, C. A.; Chameides, W. L. An Observation-Based Model for Analyzing Ozone Precursor Relationships in the Urban Atmosphere. *J. Air Waste Manage. Assoc.* **1995**, *45*, 161−180.
(19) Martin, R. V.; Fiore, A. M.; Van Donkelaar, A. Space-based diagnosis of surface ozone sensitivity to anthropogenic emissions. *Geophys. Res. Lett.* **2004**, *31*, No. L06120.
(20) Stockwell, W. R.; Kirchner, F.; Kuhn, M.; Seefeld, S. A new mechanism for regional atmospheric chemistry modeling. *J. Geophys. Res.: Atmos.* **1997**, *102*, 25847−25879.
(21) Li, M.; Zhang, Q.; Zheng, B.; Tong, D.; Lei, Y.; Liu, F.; Hong, C.; Kang, S.; Yan, L.; Zhang, Y.; et al. Persistent growth of anthropogenic non-methane volatile organic compound (NMVOC) emissions in China during 1990−2017: drivers, speciation and ozone formation potential. *Atmos. Chem. Phys.* **2019**, *19*, 8897−8913.
(22) Guenther, A.; Hewitt, C. N.; Erickson, D.; Fall, R.; Geron, C.; Graedel, T.; Harley, P.; Klinger, L.; Lerdau, M.; Mckay, W. A.; et al. A global model of natural volatile organic compound emissions. *J. Geophys. Res.: Atmos.* **1995**, *100*, 8873−8892.
(23) Lu, X.; Zhang, L.; Wang, X.; Gao, M.; Li, K.; Zhang, Y.; Yue, X.; Zhang, Y. Rapid Increases in Warm-Season Surface Ozone and Resulting Health Impact in China Since 2013. *Environ. Sci. Technol. Lett.* **2020**, *7*, 240−247.
(24) Xue, L. K.; Wang, T.; Gao, J.; Ding, A. J.; Zhou, X. H.; Blake, D. R.; Wang, X. F.; Saunders, S. M.; Fan, S. J.; Zuo, H. C.; et al. Ground-level ozone in four Chinese cities: precursors, regional transport and heterogeneous processes. *Atmos. Chem. Phys.* **2014**, *14*, 13175−13188.
(25) Li, Q.; Zhang, L.; Wang, T.; Wang, Z.; Fu, X.; Zhang, Q. "New" Reactive Nitrogen Chemistry Reshapes the Relationship of Ozone to Its Precursors. *Environ. Sci. Technol.* **2018**, *52*, 2810−2818.
(26) Chen, X.; Jiang, Z.; Shen, Y.; Li, R.; Fu, Y.; Liu, J.; Han, H.; Liao, H.; Cheng, X.; Jones, D. B. A.; et al. Chinese Regulations Are Working-Why Is Surface Ozone Over Industrialized Areas Still High? Applying Lessons From Northeast US Air Quality Evolution. *Geophys. Res. Lett.* **2021**, *48*, No. e2021GL092816.
(27) Shen, L.; Jacob, D. J.; Zhu, L.; Zhang, Q.; Zheng, B.; Sulprizio, M. P.; Li, K.; De Smedt, I.; González Abad, G.; Cao, H.; et al. The 2005−2016 Trends of Formaldehyde Columns Over China Observed by Satellites: Increasing Anthropogenic Emissions of Volatile Organic Compounds and Decreasing Agricultural Fire Emissions. *Geophys. Res. Lett.* **2019**, *46*, 4468−4475.
(28) Jin, X. M.; Holloway, T. Spatial and temporal variability of ozone sensitivity over China observed from the Ozone Monitoring Instrument. *J. Geophys. Res.: Atmos.* **2015**, *120*, 7229−7246.
(29) Air Science Group *Hong Kong Emission Inventory Report*, 2018. https://www.epd.gov.hk/epd/sites/default/files/epd/2018EmissionInventoryReport_Eng_final.pdf.
(30) Li, K.; Jacob, D. J.; Liao, H.; Shen, L.; Zhang, Q.; Bates, K. H. Anthropogenic drivers of 2013−2017 trends in summer surface ozone in China. *Proc. Natl. Acad. Sci. U.S.A.* **2019**, *116*, 422−427.
(31) Song, H.; Lu, K.; Dong, H.; Tan, Z.; Chen, S.; Zeng, L.; Zhang, Y. Reduced Aerosol Uptake of Hydroperoxyl Radical May Increase the Sensitivity of Ozone Production to Volatile Organic Compounds. *Environ. Sci. Technol. Lett.* **2022**, *9*, 22−29.
(32) Wang, N.; Lyu, X. P.; Deng, X. J.; Huang, X.; Jiang, F.; Ding, A. J. Aggravating O-3 pollution due to NOx emission control in eastern China. *Sci. Total Environ.* **2019**, *677*, 732−744.
(33) Chen, X.; Situ, S.; Zhang, Q.; Wang, X.; Sha, C.; Zhouc, L.; Wu, L.; Wu, L.; Ye, L.; Li, C. The synergetic control of NO2 and O3 concentrations in a manufacturing city of southern China. *Atmos. Environ.* **2019**, *201*, 402−416.
(34) Ren, J.; Guo, F.; Xie, S. Diagnosing ozone-NOx-VOC sensitivity and revealing causes of ozone increases in China based on 2013-2021 satellite retrievals. *Atmos. Chem. Phys. Discuss.* **2022**, *22*, 1−22.

https://doi.org/10.1021/acs.est.2c08205
Environ. Sci. Technol. 2023, 57, 109−117